Airway and parenchymal strains during bronchoconstriction in the precision cut lung slice

Document Version
Accepted author manuscript

Link to publication record in Manchester Research Explorer

Citation for published version (APA):
Hiorns, J. E., Bidan, C. M., Jensen, O., Gosens, R., Kistemaker, L. E. M., Fredberg, J. J., Butler, J. P., Krishnan, R., & Brook, B. S. (2016). Airway and parenchymal strains during bronchoconstriction in the precision cut lung slice. *Frontiers in Physiology*, *7*, [309]. https://doi.org/10.3389/fphys.2016.00309

Published in:
Frontiers in Physiology

Citing this paper
Please note that where the full-text provided on Manchester Research Explorer is the Author Accepted Manuscript or Proof version this may differ from the final Published version. If citing, it is advised that you check and use the publisher's definitive version.

OPEN ACCESS

Airway and parenchymal strains during bronchoconstriction in the precision cut lung slice

Jonathan E. Hiorns[1], Cecile M. Bidan[2, 3, 4], Oliver E. Jensen[5], Reinoud Gosens[3], Jeffrey J. Fredberg[6], Loes E. Kistemaker[3], Jim P. Butler[6], Ramaswamy Krishnan[4], Bindi S. Brook[1*]

[1]School of Mathematical Sciences, University of Nottingham, United Kingdom, [2]Laboratoire Interdisciplinaire de Physique, Université Grenoble Alpes, Centre National de la Recherche Scientifique, France, [3]Department of Molecular Pharmacology, University of Groningen, Netherlands, [4]Department of Emergency Medicine, Beth Israel Deaconess Medical Center, Harvard Medical School, USA, [5]School of Mathematics, University of Manchester, United Kingdom, [6]Department of Environmental Health, Harvard School of Public Health, USA

Airway and parenchymal strains during bronchoconstriction in the precision cut lung slice

J.E. Hiorns[†1], C.M. Bidan[†2,4,6], O.E. Jensen[3], R. Gosens[4], L.E.M. Kistemaker[4]
J.J. Fredberg[5], J.P. Butler[5], R. Krishnan[6], B. S. Brook[*1].

June 7, 2016

[†] Joint first-authors, [*] Corresponding author: bindi.brook@nottingham.ac.uk
[1] School of Mathematical Sciences, University of Nottingham, UK
[2] Laboratoire Interdisciplinaire de Physique, Université Grenoble Alpes, Centre National de la Recherche Scientifique, Grenoble, France
[3] School of Mathematics, University of Manchester, UK
[4] Department of Molecular Pharmacology, University of Groningen, Netherlands
[5] Department of Environmental Health, Harvard School of Public Health, USA
[6] Department of Emergency Medicine, Beth Israel Deaconess Medical Center, Harvard Medical School, USA

Abstract

The precision-cut lung slice (PCLS) is a powerful tool for studying airway reactivity, but biomechanical measurements to date have largely focused on changes in airway caliber. Here we describe an image processing tool that reveals the associated spatio-temporal changes in airway and parenchymal strains. Displacements of subregions within the PCLS are tracked in phase-contrast movies acquired after addition of contractile and relaxing drugs. From displacement maps, strains are determined across the entire PCLS or along user-specified directions. In a representative mouse PCLS challenged with 10^{-4}M methacholine, as lumen area decreased, compressive circumferential strains were highest in the 50μm closest to the airway lumen while expansive radial strains were highest in the region $50\text{-}100\mu$m from the lumen. However, at any given distance from the airway the strain distribution varied substantially in the vicinity of neighboring small airways and blood vessels. Upon challenge with the relaxant agonist chloroquine, although most strains disappeared, residual positive strains remained a long time after addition of chloroquine, predominantly in the radial direction. Taken together, these findings establish strain mapping as a new tool to elucidate local dynamic mechanical events within the constricting airway and its supporting parenchyma.

1 Introduction

Airway smooth muscle (ASM) cells residing within the airway wall, and the tissue in the surrounding parenchyma, are under constantly changing strains during tidal breathing. It is widely recognized that the effect of imposed strains and resulting stresses, as well as internally generated mechanical force, are of crucial importance in normal physiology and are altered in diseases such as asthma and COPD. However, while complex and inferred in organs and overly simplified in the cultured cell, their generation, transmission and transduction in the settings of an intact airway remain difficult to measure. Indeed, there are currently no straightforward approaches to quantify the strains or stresses acting on cells and tissues in their native airway microenvironment. In the absence of such knowledge, the mechanical interactions involved in airway (patho)physiology will remain poorly understood.

A well-established experimental preparation for studying airway reactivity, and corresponding biomechanical response, is the precision-cut lung slice (PCLS) (e.g. [23, 30, 29]). The key advantage of the PCLS is that vital functional interactions between airways, arterioles, and veins are preserved within the alveolar parenchyma [25]. Additional practical considerations include its ease of preparation, ease of storage via cryopreservation [24, 3], widespread applicability to many animal species [28] including humans [32], and suitability for high-resolution imaging of molecular dynamics [25]. In the PCLS, responses to electric field stimulation [27, 26] and mechanical stretch [10, 18, 11] have also been ascertained, highlighting the physiological relevance of this system.

Biomechanical data from PCLS studies, to date, have largely focused on changes in airway caliber. These datasets, however, contain a rich source of additional dynamic and spatial biomechanical data that heretofore have not been investigated. For example, a limited number of studies have utilized the PCLS to examine the mechanical interdependence between the constricting airway and the surrounding parenchyma [1, 9, 19]. However, beyond the immediate vicinity of the contracting airway, the parenchyma contains other

airways and arterioles which may themselves contract or even passively contribute to the effective material properties of surrounding tissues. Accordingly, detailed spatio-temporal maps of tissue deformation are necessary to elucidate the biomechanical aspects of airway-parenchymal interactions and the inherent transmission of force.

Here, we describe the development and implementation of a strain mapping tool that provides spatial and temporal data from PCLS video recordings. In a representative mouse PCLS they revealed heterogeneous strain profiles around distinct structural features that surround the contracting airway. These heterogeneities highlight the possibility of distinct micromechanical environments for resident cells so that cells may in turn respond heterogeneously depending on their location [7]. Furthermore, the present analysis technique promises to be highly useful in correlating levels of strain and structural remodeling in the airway and surrounding parenchyma.

2 Methods

2.1 Precision cut lung slice preparation and contraction experiment

2.1.1 Animals

Homozygous, inbred, specific-pathogen-free breeding colonies of C57Bl/6NTac wild-type mice were obtained from Taconic. Animals were housed conventionally under a 12-h light-dark cycle and received food and water *ad libitum*. All experiments were performed in accordance with the national guidelines and approved by the University of Groningen Committee for Animal Experimentation (DEC5463I and DEC6792A).

2.1.2 Precision-cut lung slices

Mouse PCLS were prepared according to a protocol described previously for guinea pig PCLS [22]. Male C57Bl/6 mice (6-8 weeks old) were euthanized by intraperitoneal pento-barbital injection (400 mg/kg, hospital pharmacy, University Medical Center Groningen), after which the lungs were filled with 1.5 mL low melting-point agarose solution (1.5% final concentration (Gerbu Biotechnik GmbH, Wieblingen, Germany) in CaCl2 (0.9mM), MgSO4 (0.4 mM), KCl (2.7 mM), NaCl (58.2 mM), NaH2PO4 (0.6 mM), glucose (8.4 mM), NaHCO3 (13 mM), Hepes (12.6 mM), sodium pyruvate (0.5 mM), glutamine (1 mM), MEM-amino acids mixture (1:50), and MEM-vitamins mixture (1:100), pH=7.2). The agarose was solidified for 15 minutes, by placing the lungs on ice and at 4°C. Lungs were harvested and individual lobes were sliced at a thickness of 250 μm in medium composed of CaCl2 (1.8mM), MgSO4 (0.8 mM), KCl (5.4 mM), NaCl (116.4 mM), NaH2PO4 (1.2 mM), glucose (16.7 mM), NaHCO3 (26.1 mM), Hepes (25.2 mM), pH = 7.2, using a tissue slicer (Compresstome^{TM} VF-300 microtome, Precisionary Instruments, San Jose CA, USA). Thereafter, slices were kept at 37°C in a humidified atmosphere of 5% CO_2 and washed every 30 minutes for four times to remove the agarose and cell debris in medium composed of CaCl2 (1.8mM), MgSO4 (0.8 mM), KCl (5.4 mM), NaCl (116.4 mM), NaH2PO4 (1.2 mM), glucose (16.7 mM), NaHCO3 (26.1 mM), Hepes (25.2 mM), sodium pyruvate (1mM), glutamine (2 mM), MEM-amino acids mixture (1:50), MEM-vitamins mixture (1:100,) penicillin (100 U/mL) and streptomycin (100 μg/mL), pH = 7.2.

2.1.3 Contraction studies

The response of lung slices were recorded after addition of the contractile agonist metha-choline (MCh; 10^{-4}M, ICN Biomedicals, Zoetermeer, the Netherlands) at $t_0 = 0$ s, and then addition of the bitter taste receptor agonist chloroquine (ChQ; 10^{-3}M, Sigma-Aldrich, Zwijndrecht, The Netherlands) to induce relaxation at $t_1 = 600$ s (in the presence of MCh). As described previously, a nylon mesh and a metal washer were used to keep the lung slice in place. Bright field images of the lung slices were captured in time-lapse (1 frame per 2 seconds) with a resolution of 1280x960pxl (1.15 m/pxl) using an inverted microscope (Eclipse, TS100; Nikon). Airway luminal area was quantified using image acquisition software (NIS-elements; Nikon).

2.2 Strain and displacement maps using image analysis

This section details the determination of 2-dimensional time-dependent displacement and strain maps from video sequences of mouse PCLS. In order to calculate displacement and strain fields in a given video frame at a given time point, a number of computational algorithms were developed; the overview of the whole method is shown in Fig. A-1 and Fig. A-2 in the Appendix, as well as further details of the algorithms.

2.2.1 Displacement fields

First, the frames were pre-processed with MATLAB to set the length scale in μm and stretch the range of pixel densities so that specific features became more prominent. This pre-processing step gave a list of the frame numbers and a series of images corresponding to adjusted frames. Second, the Farnebäck algorithm [12] as implemented in C++ / OpenCV was used to calculate an estimate of the displacement vector between an initial (or reference) and final image (the frame of interest) for each of the pixels. Then, strain matrices were determined at equally spaced points chosen across the image. To do so, four displacement vectors around the point of interest and central difference methods were used to calculate derivatives in the horizontal and vertical directions from which the major and minor eigenvectors and eigenvalues of the strain matrix were evaluated. The initial coordinates of the selected points, the components of the displacement vectors, the major and minor strain eigenvalues and the components of the major strain eigenvector were saved to be used in post-processing. This sequence was repeated for each frame of interest.

Finally, displacements and strains were displayed with MATLAB and their value was set to zero where there was no tissue. Displacement plots could either show arrows on a bright field image (initial or final) or display the magnitude of the displacements in color maps. Major (radial) and minor (circumferential) strain eigenvalue distributions were also displayed as color maps.

2.2.2 Determining strain fields from displacement fields

An alternative to plotting displacement fields is to plot strain fields. An advantage of analyzing strains over displacements is that, if there is movement of a lung slice (relative to the camera position) that is not related to the contraction of the airway, the displacement field will be affected, but the strain field will not.

We assume that displacements between two frames are known (as determined previously), where the coordinates are denoted (X, Y) in the first image and (x, y) in the second

image. The deformation gradient tensor is given by

$$\mathsf{F} = \left(\begin{array}{cc} \frac{\partial x}{\partial X} & \frac{\partial x}{\partial Y} \\ \frac{\partial y}{\partial X} & \frac{\partial y}{\partial Y} \end{array} \right). \tag{1}$$

The Lagrangian strain tensor is defined as $\mathsf{E} \equiv (\mathsf{C} - \mathsf{I})/2$, where $\mathsf{C} \equiv \mathsf{F}^T \mathsf{F}$ is the right Cauchy-Green deformation tensor. Thus,

$$\mathsf{E} = \left(\begin{array}{cc} E_{11} & E_{12} \\ E_{12} & E_{22} \end{array} \right) = \left(\begin{array}{cc} (\frac{\partial x}{\partial X})^2 + (\frac{\partial y}{\partial X})^2 - 1 & \frac{\partial x}{\partial X}\frac{\partial x}{\partial Y} + \frac{\partial y}{\partial X}\frac{\partial y}{\partial Y} \\ \frac{\partial x}{\partial X}\frac{\partial x}{\partial Y} + \frac{\partial y}{\partial X}\frac{\partial y}{\partial Y} & (\frac{\partial x}{\partial Y})^2 + (\frac{\partial y}{\partial Y})^2 - 1 \end{array} \right) /2. \tag{2}$$

One way to visualise the strain is to find the eigenvalues and eigenvectors of E so that the magnitude and direction of the principal strains can be plotted. The characteristic polynomial for the tensor is

$$\lambda^2 - (E_{11} + E_{22})\lambda + (E_{11}E_{22} - E_{12}^2) = 0, \tag{3}$$

with coefficients given by the strain invariants $I_1 = E_{11} + E_{22}$ and $I_2 = E_{11}E_{22} - E_{12}^2$. Solving the characteristic polynomial yields the eigenvalues in terms of the invariants,

$$\lambda^{\pm} = \frac{I_1 \pm \sqrt{I_1^2 - 4I_2}}{2}. \tag{4}$$

The eigenvalues depend on a combination of the invariants and so are independent of the coordinate system used. Now

$$I_1^2 - 4I_2 = (E_{11} - E_{22})^2 + 4E_{12}^2 \geq 0, \tag{5}$$

so in general there are two real eigenvalues. The only exception is when $E_{11} = E_{22}$, for which there is a repeated eigenvalue.

To find the eigenvectors the following equation must be solved:

$$\left(\begin{array}{cc} E_{11} - \lambda^{\pm} & E_{12} \\ E_{12} & E_{22} - \lambda^{\pm} \end{array} \right) \left(\begin{array}{c} x \\ y \end{array} \right) = \left(\begin{array}{c} 0 \\ 0 \end{array} \right). \tag{6}$$

From the first row, the unit eigenvectors satisfy

$$\frac{(E_{12}, \lambda^{\pm} - E_{11})}{\sqrt{E_{12}^2 + (\lambda^{\pm} - E_{11})^2}}.$$

The second row provides an equivalent relationship. The eigenvector could equally point in the opposite direction. The sign of the corresponding eigenvalue can be used to determine if the strain is expansive ($\lambda > 0$) or compressive ($\lambda < 0$). We assumed that for a single contracted airway, a component of the major principal strain points towards, rather than away from, the lumen. In all our results we found that our principal directions were essentially radial and circumferential; here on we therefore refer to these as radial and circumferential directions.

2.3 Radial profiles of strain

2.3.1 Strain kymographs

The strain values plotted as maps were averaged along the circumferential direction as a function of the distance to the airway edge. Each frame of the sequence was made binary with the lumen in white (1) and the rest in black (0) and resized so as to match the dimensions of the corresponding strain maps. For each pixel out of the airway (0), the distance to the nearest airway pixel (1) was computed and stored in a matrix of the same dimension as the ones containing the radial and circumferential strain values. The distance/strain couples were then sorted in distance bins of 15μm and the mean of the corresponding strain values for this bin was calculated. The results were then represented as series of line plots of the mean strain average as a function of the distance to the airway, time being represented by the color code of the lines. Alternatively a form of kymograph was plotted with the strain represented as a function of time on the x-axis and the distance to the airway on the y-axis; the value of the strain was color-coded at the corresponding coordinates. This graphic representation highlights how the strains were altered during and after airway contraction and relaxation.

2.3.2 Spokes analysis

An alternative to finding strain fields across the whole image was to determine the strains only at a selection of points along vectors normal to the lumen. To do this, the lumen area of airway in the image had to be identified first. An ellipse was fitted to the lumen of the airway in the first frame. Two methods were used to estimate the position of the lumen and the best result was chosen (A-1.2.1 in the Appendix). The area around the airway was split into eight regions, within which we selected seven sets of points radiating out from the lumen; multiple sets of points were used so that the average strain and variability could be determined as a function of distance from the lumen.

The Farnebäck algorithm (A-1.2.2 in Appendix) was used to determine the displacements in the radial and circumferential directions at each point and these values were averaged within each of the sections for each radial position, in order to remove small errors.The coordinates of four neighbouring points were then determined for each of the points on the spokes. These were selected based on being a specific distance away in the x or y direction. However, the coordinates of these surrounding points were unlikely to be at integer values of pixels, in which case bilinear interpolation of the displacement of the four closest pixels was used first to calculate estimates for the displacements at the surrounding points, then to derive the strain matrix (using central difference methods to calculate derivatives) and finally the mean of the radial and circumferential strain eigenvalues in each section. MATLAB was used to plot graphs of the section-averaged strain as a function of distance from the lumen, which could also be used to show how the time-dependent distribution of average strain alters as the airway contracts.

3 Results

3.1 Strain maps show global spatio-temporal influence of airway smooth muscle contraction on the airway wall and parenchyma

Bronchoconstriction in response to 10^{-4}M methacholine (MCh), followed by relaxation in response to 10^{-3}M Chloroquine (ChQ) (in the presence of MCh) were recorded by
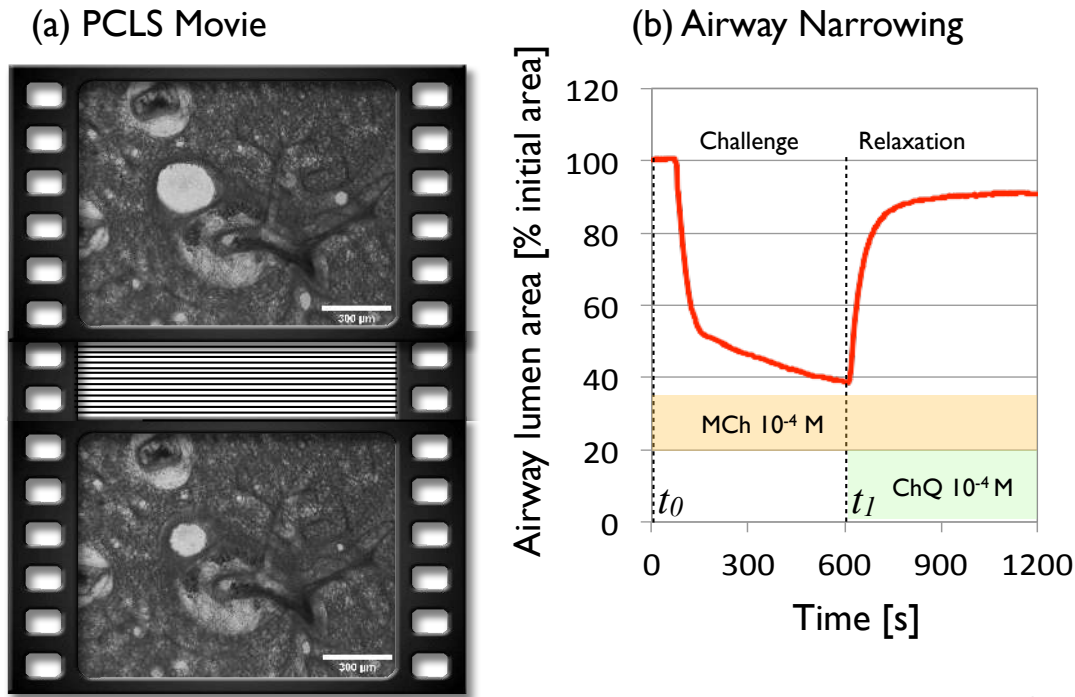
6

Figure 1: Global analysis of the deformations of a $250\mu m$ mouse lung slice during agonist driven contraction with methacholine (10^{-4}M) and subsequent bitter taste receptor agonist relaxation with chloroquine (10^{-3}M), reveals the global behavior of the parenchyma. (a) Two frames of a phase contrast PCLS movie selected before ($t_0 = 0$s) and after contraction ($t_1 = 600$s). (b) Airway calibre plotted as a function of time during contraction and relaxation.

phase contrast microscopy with example images before and at maximal contraction shown in Fig. 1(a). The time-dependent change in cross sectional area of the airway (Fig. 1(b)) matched previously measured airway profile changes (e.g. [5, 30]), demonstrating features previously pointed out by Bergner and Sanderson [5] with an initial steep phase of fast narrowing, followed by a slower, asymptotic phase. We note that in this particular strain of mice, maximal MCh-induced airway narrowing, as measured by luminal area, was achieved only on addition of 1mM methacholine, although airway closure is nearly maximal at 0.1 mM (Fig. S1) in Supplemental Material). Addition of ChQ in the presence of MCh induced complete bronchodilation in a series of experiments as shown in Fig S2 (Supp. Mat.).

Local displacement of small regions (7x7 pixels), computed with respect to a reference image (at t_0 right before the challenge) are displayed using displacement vectors in Fig. 2(a) 10 min after MCh challenge. These are overlaid on top of the image of the contracted airway, with the boundary of the airway before contraction represented as a white dotted line. As expected, these displacement vectors are oriented towards the centre of the lumen. A map of displacement magnitude over the entire PCLS (Fig. 2(b)) indicates, however, that although the largest displacements are in or near the airway wall, there are significant non-zero displacements almost 2 airway-diameter lengths away from the airway wall (to the left of the airway in (Fig. 2(b)).

Tissue displacements, observed in Fig. 2(b), are determined for the whole image and

7

Displacement maps
(a) Vectors
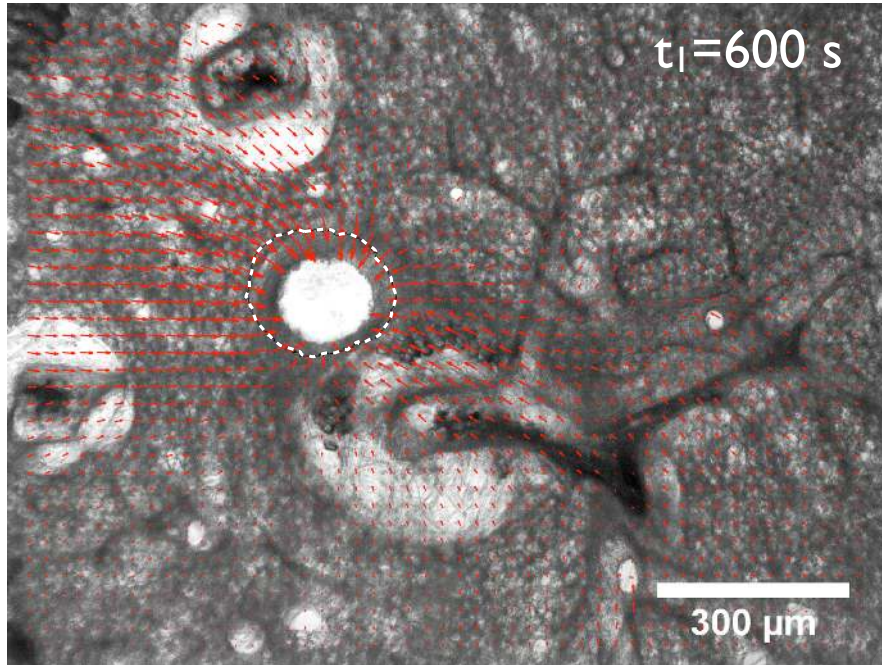
(b) Magnitude (μm)

Figure 2: Global analysis of the deformations of the mouse lung slice in Fig. 1. Displacement (a) vectors and (b) magnitude of small regions (7x7pixels) of the slice computed between the reference (at t_0) and the contracted state (at t_1). The boundary of the airway before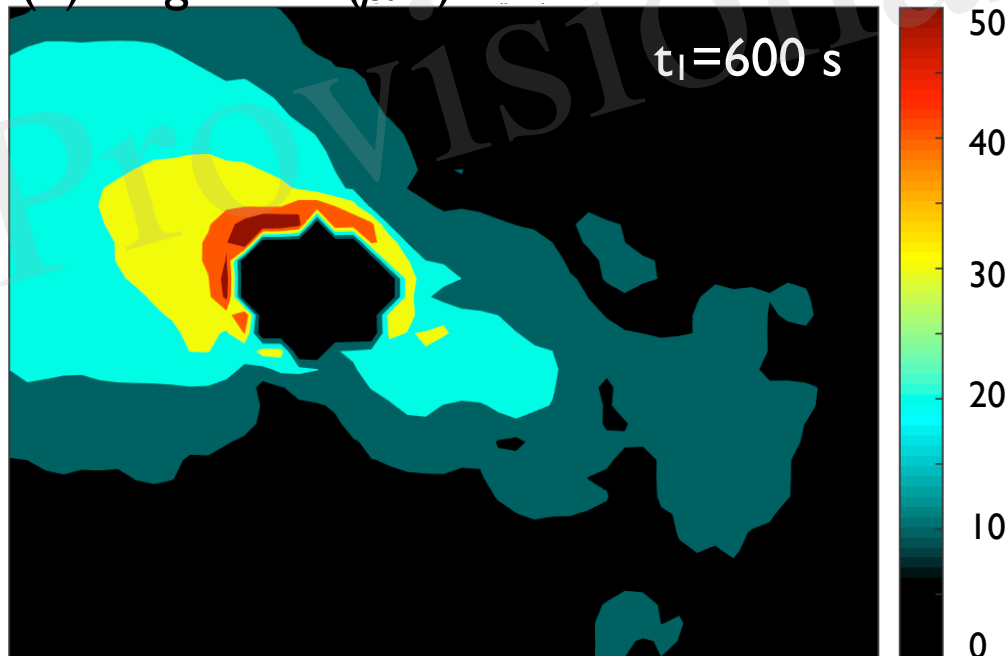 contraction is represented as a white dashed line. See movies M1 and M2 (and Figs. S3-S5 for analyses of additional PCLS) in Supplemental Material.
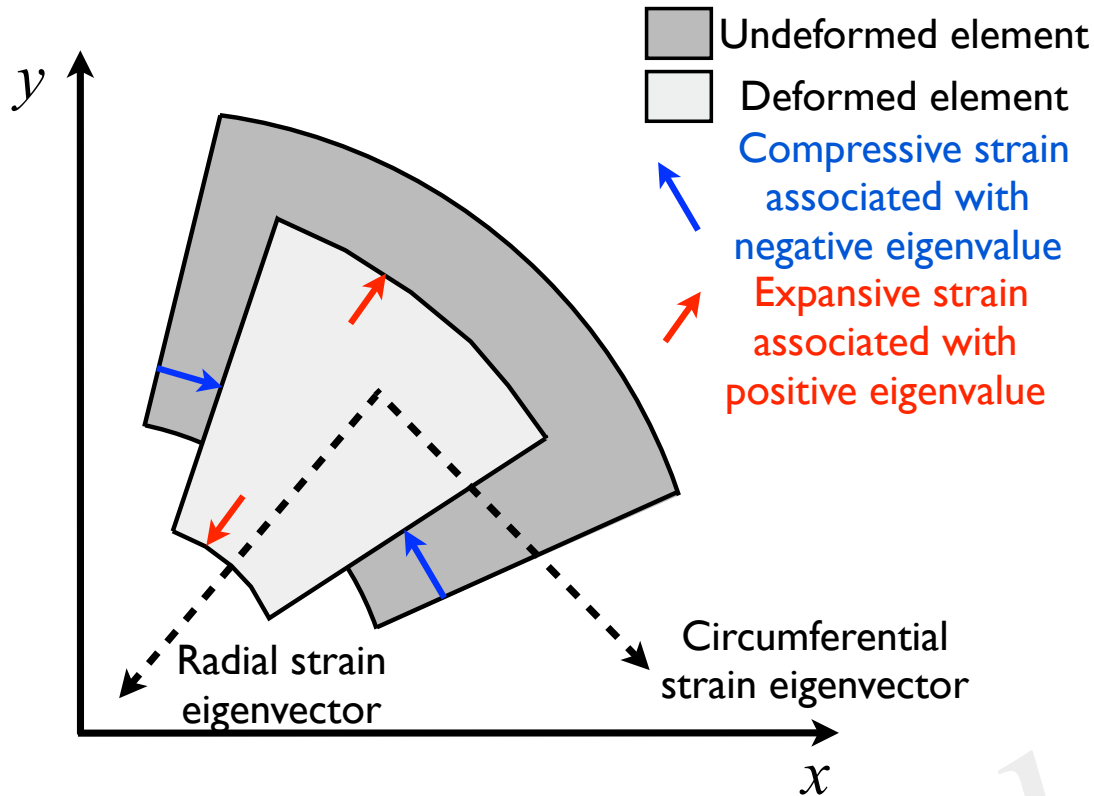
Figure 3: Schematic illustrating effect of contraction on an element of tissue in the PCLS. Strains are decomposed into radial and circumferential components associated with eigenvectors that essentially point in the radial and circumferential directions. Determination of these eigenvector directions allows the deformation to be described predominantly as expansion and compression with minimal shear (diagonal elements in the strain tensor, E_{11} and E_{22} in (2), dominate over the off-diagonal elements, E_{12}).

normalized to obtain strain maps. The major and minor strains approximately represent the radial and circumferential strains respectively (Fig. 3). We observe that their spatial distributions are clearly quantitatively and qualitatively different (Fig. 4). In particular we note that the deformations in the radial directions are essentially stretches ((Fig. 4(a); positive major strains) whereas the deformations in the circumferential directions are largely compressive (Fig. 4(b); negative minor strains). In both cases, the largest deformations are found along the airway wall, but hot spots of strains are also present in the parenchyma. Fig. 5(right) highlights the heterogeneous distribution of the deformations over the parenchyma surrounding the airway, with some regions being dominated by extension/stretch and others by compression.

To visualize the temporal evolution of strain distribution, the displacements and strain maps were computed for each frame of the 20min contraction and relaxation movie, with respect to the reference image at t_0 (see movies in Supplementary materials). For each time point, major and minor strains are averaged circumferentially over pixels that are radially equidistant (at 15μm intervals) from the airway wall and plotted along the radial direction for each time point and superimposed on Fig. 5 (left column). Again, the peaks of strain are found in the 100μm region closest to the airway wall, with the radial strain being mainly positive (expansive) and the circumferential strain negative (compressive). The strain profiles however, show that compression dominates in the 50μm closest to the

(a) Radial Strain   **(b) Circumferential Strain**   Strain
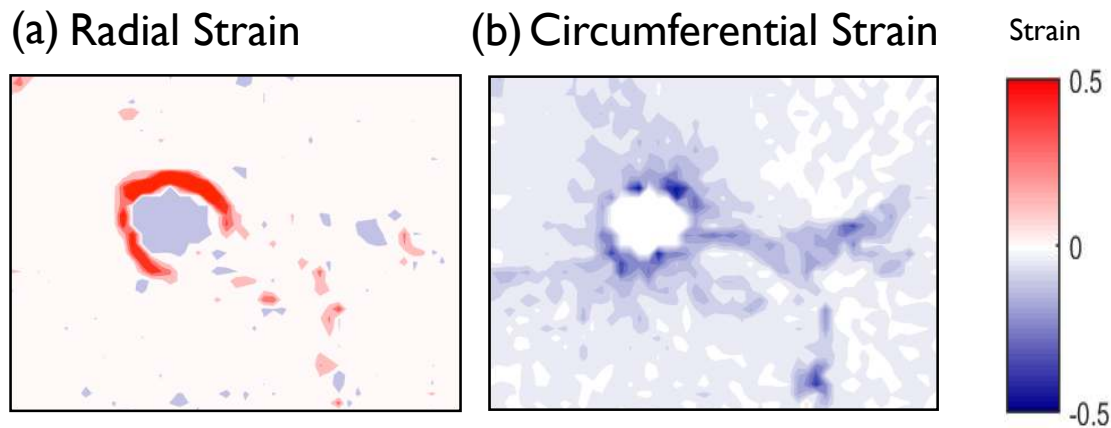
Figure 4: Global analysis of the deformations of the mouse lung slice in Fig. 1. Radial (major) and circumferential (minor) strains calculated by spatial derivation of the displacements and displayed as maps over the whole field. See movie M3 (and Figs. S3-S5 for analyses of additional PCLS) in Supplemental Material.
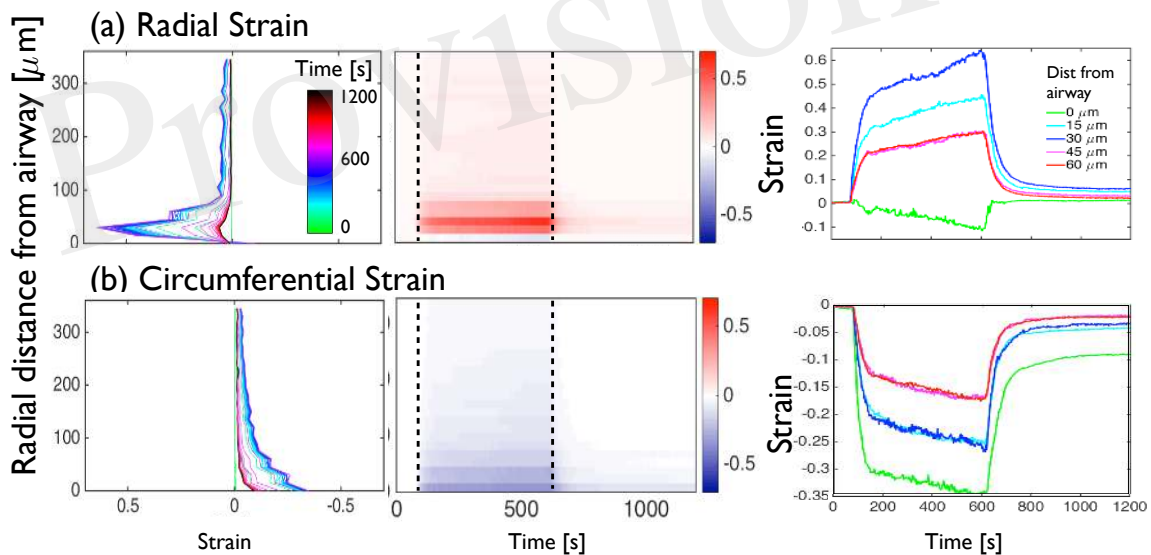
Figure 5: Global analysis of the deformations of the mouse lung slice in Fig. 1. Temporal evolution of (a) radial and (b) circumferential strains as a function of distance from the airway. Left column: superimposition of distance-strain line plots for increasing time as indicated by the colorbar (inset on top figure of left column). Middle column: adapted kymographs showing magnitude of strain, as indicated by the colorbar to the right of each figure. Right column: superimposition of line plots showing temporal evolution of strain at 0, 15, 30, 45 and 60 μm from the airway lumen.
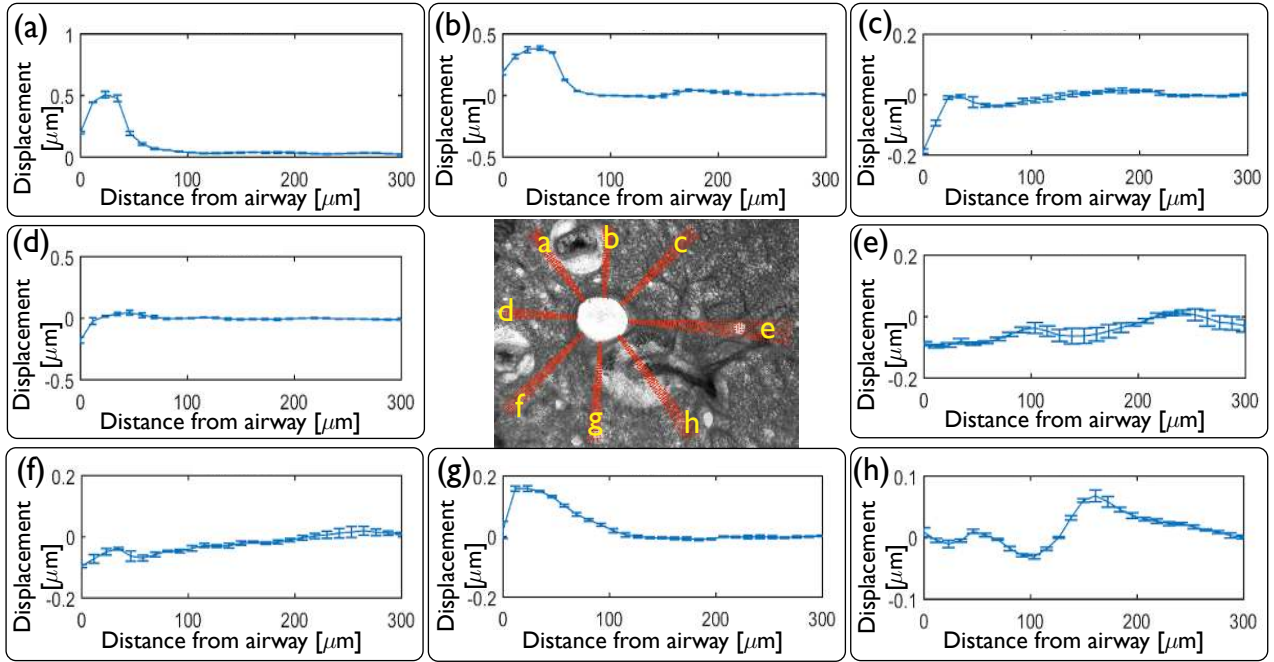
Figure 6: Local quantitative analysis of the mouse lung slice (central image) from Fig. 1 at peak contraction following application of agonist. Inward radial displacements are plotted as a function of distance from the airway lumen for each of the 8 sets of independent spokes (**a** - **h**) shown on the central image. Spokes **a**, **b** and **g** go through the highly collagenous part on the edge of a blood vessel; spokes **c**, **d** and **f** go through alveolar tissue, spoke **e** intersects another small contractile airway and **h** goes through a blood vessel.

airway lumen whereas stretch dominates between 50 and $100\mu m$ away from the lumen edge. The colour code used to represent the time indicates that in all cases, the strain magnitudes progressively increase until the addition of relaxant at $t_1 = 600$ s.

To better visualize the evolution of the strain profiles, the data are represented as ky-mographs (Fig. 5(middle column)). We observe that at 90s, after the contraction starts, both radial and circumferential strains over the entire PCLS indicate that the large defor-mations observed in the vicinity of the airway wall propagate further away. Aligning the 2D plots with the standard contraction curve (Fig. 1(b)) enables us to (i) correlate the lag time with the absence of deformation, (ii) correlate the early phase of fast narrowing with the rapid appearance of deformations in the $100\mu m$ closest to the airway lumen, (iii) ob-serve the slower asymptotic phase of contraction from 400 to 600s and (iv) correlate the rapid attenuation of the majority of strain with addition of relaxant added after 600 s.

Plotting the strains at specific distances from the lumen as a function of time (Fig. 5 (right column)), we observe that there is some compressive radial strain at the lumen (green curve; Fig. 5(a) (right column)) which is not visible in the left panel. Additionally we observe that although the radial strains return to zero at the lumen upon addition of ChQ (green curve, 0 μm), the regions further away from the lumen (blue curve, 30 μm) retain a residual positive major strain a long time after relaxant ($t = 1200s$) was added, suggesting some longer term structural changes. Furthermore, the circumferential strain remained significantly compressive at the lumen, and to a lesser extent further away from the lumen, at $t = 1200s$.

11
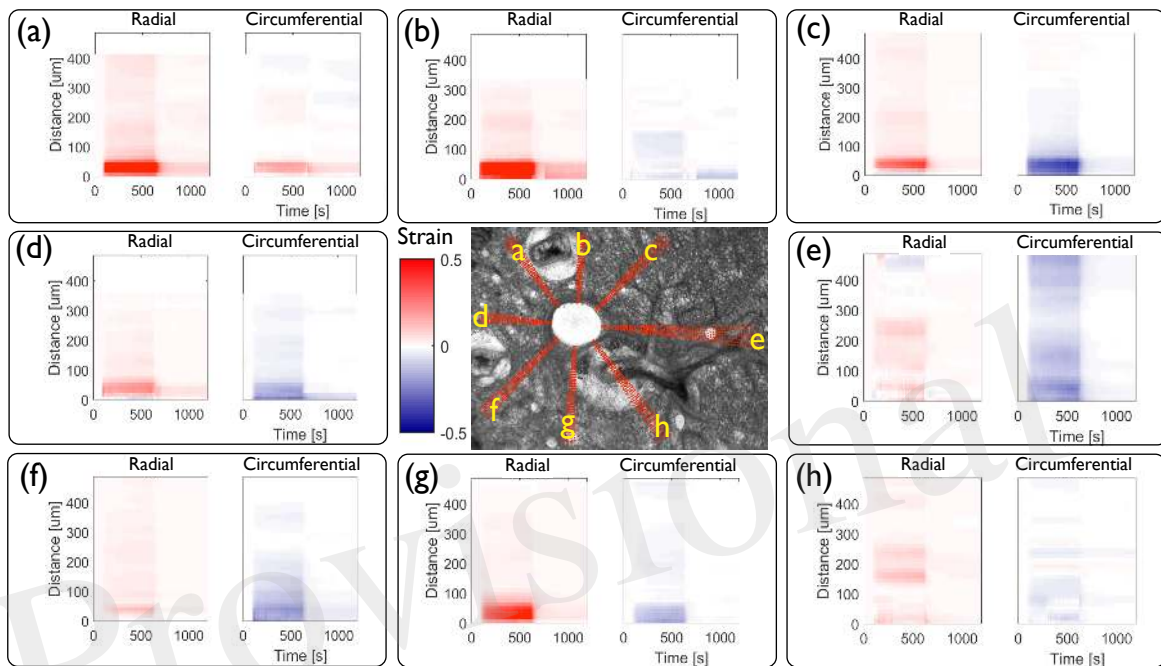
Figure 7: Local quantitative analysis of a mouse lung slice (central image) from Fig. 1 during agonist driven contraction. Radial and circumferential strain kymographs are plotted as a function of both time and distance from the airway lumen for each of the 8 sets of independent spokes (**a** - **h**) shown on the central image. Spokes **a**, **b** and **g** go through the highly collagenous part on the edge of a blood vessel; spokes **c**, **d** and **f** go through alveolar tissue, spoke **e** intersects another small contractile airway and **h** goes through a blood vessel.

3.2 Spokes analysis reveals the influence of structural heterogeneities on strain distribution in the airway wall and parenchyma

As an alternative to computing the displacements and strains across the whole field, we compute displacements and strains along eight sets of spokes normal to the airway wall (Fig. 6(center)). Displacements averaged over each set of spokes at maximum contraction, at t_1 (Figs. 6(a-h)), reveal the heterogeneity observed in Fig. 2. Within each set of spokes, we observe very small variability (as indicated by the error bars on each line plot in Fig. 6(a-h)) but significantly different displacement profiles around the airway.

From these displacements we determine the time evolution of radial and circumferential strain profiles in all directions and represent them as kymographs in Fig. 7. As the parenchymal tissue is structurally heterogeneous, the spokes selected around the airway intersect different structural features and hence display different strain profiles. While most of these features are physiological, some of them are modified during the slicing procedure. For instance, blood vessels are known to contract strongly in response to the slicing, disrupting the rather weak connective tissue tethering the blood vessel to the parenchyma, leaving behind spaces that appear to be filled by agarose. The strains along three spokes going through the agarose surrounding the blood vessels (a, b, g) show high positive radial strains characteristic of large stretch in the close vicinity of the airway lumen. Three spokes that intersect only alveolar tissue (c, d, f), display roughly similar magnitudes of radial and circumferential strains during the entire contraction event. The spoke (e) intersects another smaller contractile airway, which greatly affects the corresponding strain profile in spatially distributing the deformations between the main and the secondary airway, with a slight domination of compression which persists as far as $400\mu m$ from the lumen. In contrast, the spoke (h) passes through an adjoining blood vessel surrounded by agarose, which also smooths the strain profile. During the relaxation phase, most of the strains disappear, except in the spokes (a,b,g). Along these, one can observe residual positive strains, predominantly in the radial direction. This suggests that the circumferentially averaged positive residual strains observed above (Fig. 5 (right column)) can be attributed specifically to positive residual strains in this region of the tissue. Taken together, the strain profiles show that the extent to which strain is transmitted from the contractile airway towards the parenchyma depends highly on the structural heterogeneities present around the airway (be they physiological or experimentally-induced).

4 Discussion

To date, most studies using PCLS have simply monitored airway caliber. Although a few studies have extracted some detailed strain data from PCLS [1, 9, 19], these have been obtained by tracking specific landmarks in the tissue. In this study, by contrast, we present a computational strain-mapping tool that is able to characterize heretofore inaccessible mechanical events that bear directly upon the physiology of airway narrowing. In a representative mouse PCLS, we illustrate how a variety of displacement and strain measures can be visualized dynamically and quantitatively in both the contracting airway and the surrounding parenchymal tissue.. Displacements of sub-regions of the slice are tracked on the phase contrast movies acquired after addition of contractile and/or relaxing drugs to generate maps of displacement across the whole slice. Sequences of strain maps or maps of normalized deformations are then derived from the displacement maps. With our computational strain-mapping tool, we provide access to the detailed mechanical response data in PCLS in the whole airway-parenchymal tissue both globally and also along local

user-specified directions. The strain maps give an overview of the deformations imposed by ASM contraction on the airway wall, the tethers and the alveolar tissue. At maximum contraction, both radial and circumferential strains are higher in the airway wall and on the tethers. However, the maps reveal that these deformations are partly transmitted through the slice and that their distribution in the parenchymal tissue is highly heterogeneous. Strain data are thus treated at two different scales so as to derive global and local behaviors of the tissues in response to ASM contraction.

We first extracted the global behavior of the radial and circumferential strain profiles as a function of both time and space (Fig. 4). In the present representative mouse slice, the maximum deformation appears at the airway lumen, where the airway smooth muscle is located (due to contraction, triggered by methacholine), about 1min after addition of the contractile agonist, and essentially manifests as a radial expansion and a circumferential compression. In the radial direction, a sharp drop in strain is observed, starting from 120μm away from the airway lumen, but the non-zero strain values observed at larger distances from the lumen indicate that deformations are partially transmitted to the parenchymal tissue during bronchoconstriction (Fig. 5). After addition of the bitter taste receptor agonist, chloroquine, to relax the ASM cells, the small strains quickly disappear in the parenchyma but a residual radial stretch remains in the airway smooth muscle even after 10min. This sustained mechanical response is completely missed if only the airway calibre is measured.

We also extracted the local displacement (Fig. 6) and strain profiles as a function of time and space (Fig. 7) in order to investigate the heterogeneities revealed by the strain maps. These heterogeneous patterns are likely to be linked to the mechanical and structural heterogeneities of the underlying tissue. Indeed, stiffer tissue is subject to relatively small deformations, relatively high stresses and transmits the force generated by the contractile ASM, whereas softer tissue is subject to large deformations and cannot transmit the same levels of force. Furthermore, other contractile airways in the neighborhood of the airway of interest affect the strain distribution as they contribute to additional load and stiffer tissue. This structural aspect is striking in this representative mouse slice (Fig. 7), where three blood vessels and a smaller contractile airway surround a large bronchial airway. Strain profiles computed in spokes that traverse these particular features of the tissue, show very different behavior. It is also possible that the strain profile depends on a possible heterogeneous distribution of ASM bundles around the airway lumen; the larger strains observed in the upper left part of the tissue adjacent to the airway may be due to larger amounts of ASM there than in the lower part of the airway. In any case these heterogeneous strain profiles (that emerge from the integrative response of both force generation and locally variable stiffnesses [16]) are likely to provide distinct micromechanical environments for resident cells that may in turn respond heterogeneously depending on their location [7].

As with many image analysis methods, robust mechanical studies on PCLS require samples and contraction experiments of high quality. Therefore, strain map users have to be aware of the limitations associated with both PCLS harvesting and image acquisition during contraction experiments when interpreting the results. For example, the vascular smooth muscle in blood vessels are known to spontaneously contract before the slicing process, which causes disruption of tethers connecting blood vessels to surrounding parenchymal tissue which show up in the image as large white areas filled with agarose (Fig. 2(a)). Agarose being relatively stiff compared to the rest of the alveolar tissue, the positive major strains (predominantly stretch in the radial direction) indicate that tissue is rather squeezed between the airway wall and the edge of the large agarose area, whereas the negative minor strains (compression in the circumferential direction) are also observed in the center of the collapsed blood vessels (Fig. 7). The artificial presence of agarose around the blood vessels in the tissue thus generates strain patterns that are likely not physiologically relevant

in vivo. Injection of gelatin into the vasculature during lung harvesting may prevent this phenomenon [30, 23]. Additionally the presence of agarose in the parenchymal spaces will contribute viscoelastic components not ordinarily present *in vivo* [9, 19] thus modifying effective mechanical properties and dynamic response of the parenchymal tissue. It is also vitally important to ensure that the edges of the PCLS during the contraction experiment are held down to prevent sliding of the slice and therefore control the boundary conditions of the system. This is currently done with a mesh and a washer. Acquiring the contraction movie with high resolution and low magnification is preferable in order to capture enough of the parenchymal tissue surrounding the airway of interest. Although strain maps can be derived from any set of contraction images as illustrated in additional examples in the Supplemental Material (Figs S3-S5) the significant structural variability seen in all the PCLS has precluded the derivation of a single global metric that can capture the different strain distributions observed around just one airway. Finally, our approach for image analysis was developed and validated specifically on bright-field images. In future, we intend to expand its use to phase contrast images that have significantly higher contrast and increased clarity.

The mechanisms of bronchodilator-induced airway dilation, including the intracellular signaling events that these substances activate in the ASM cells or lung tissue, are likely to vary between each class of bronchodilator and are different to those that cause airway dilation due to bronchoconstrictor degradation (e.g., by esterases in the tissue) or withdrawal. However, our primary aim was to demonstrate how our computational tool allows us to assess residual strains after a full cycle of constriction and dilation, regardless of the underlying chemical pathways that have induced them. Indeed these data remain to be verified more broadly with other bronchodilator pathways in future studies.

Methods for determination of local tissue distortions have been previously developed by Malcolm et al. [20] and used in some PCLS studies (e.g. [1, 9, 19]). This technique, mentioned above, requires identification of visually obvious anatomical landmarks around the image, the changing positions of which are then tracked through the sequence of images until contraction is complete; displacement vectors are then determined between the start and end positions of the landmark. The technique we have exploited and further developed, however, is able to determine the displacement vectors and strain fields over the entire image without need to select landmarks, allowing for more systematic interrogation of the underlying data (such as through the spokes analysis we have developed). A similar strain-mapping technique was used by West et al [31] to characterize strains in a tissue-engineered airway smooth muscle.

We also expect this strain-mapping tool to have application in other PCLS studies aimed at understanding airway mechanics. For example, Lavoie et al. [18] addressed the role of transpulmonary pressure variations on bronchoconstriction by adapting cell mapping rheometry for use with PCLS. Such studies can benefit from strain mapping; first to calibrate the stretch device through a precise measurement of the strains imposed on the soft substrate; then to quantify the deformations of the PCLS in response to those strains. The predictive capabilities of computational models, developed to understand airway tissue mechanics (e.g. [15]) and airway-parenchymal interdependence [19], can be further enhanced by quantitative validation using additional data provided by the strain-mapping method.

Further work is required to investigate whether residual strains observed are due to sustained mechanical change or length adaptation. If present *in vivo*, this is likely to trigger mechanotransduction pathways responsible for longer term modification of cellular and extracellular properties as well as structural changes termed airway remodeling [21]. Such remodeling of the airway smooth muscle compartment is a hallmark of lung diseases such as asthma [17, 8, 13] and COPD [6]. When combined with biological markers of remodeling (such as contraction-driven activation of TGF-β [22, 2]), the present analysis technique

promises to be highly useful in correlating levels of deformations and remodeling in the airway and surrounding parenchyma. Internal stresses in response to tissue strains, which are experimentally inaccessible but can be predicted using validated models [16], will play an important role in understanding the nature of the micromechanical environment *in vivo*.

Many lung diseases such as asthma and COPD are characterized by airway hyper-responsiveness and structural changes in the airway (remodeling) or the parenchymal tissue (emphysema). We believe the strain-mapping tool we have developed could enable characterisation of the mechanical aspects of such pathophysiology in human PCLS. The evident wide use [14, 32, 4, 10, 25, 27, 26, 28, 18, 11], and need to characterize the mechanics of airway tissue, [1, 9, 19] suggests that making the strain mapping computational tool widely available will benefit researchers within the airway smooth muscle, asthma and COPD communities. Moreover, the method proposed in this work can be easily adapted to any other type of precision cut slices focusing on contracting hollow organs like the gut, bladder, uterus, or the vascular system, and the associated pathologies related to their contractile behavior.

Funding

Acknowledgements

References

[1] A. Adler, E.A. Cowley, J.H.T Bates, and E.H Eidelman. Airway-parenchymal inter-dependence after airway contraction in rat lung explants. *Journal of Applied Physiology*, 85:231–237, 1998.

[2] Tatler A.L., John A.E., Jolly L., Habgood A., Porte J., Brightling C., A.J. Knox, L. Pang, D. Sheppard, X. Huang, and G. Jenkins. Integrin αvβ5-mediated tgf-β activation by airway smooth muscle cells in asthma. *J Immunol*, 187:6094e107, 2011.

[3] Y. Bai, N. Krishnamoorthy, K. R. Patel, I. Rosas, M. J. Sanderson, and X. Ai. Cryopreserved human precision-cut lung slices as a bioassay for live tissue banking: a viability study of bronchodilation with bitter-taste receptor agonists. *Am J Respir Cell Mol Biol*, 10.1165/rcmb.2015-0290MA, 2015.

[4] Y. Bai and M. J. Sanderson. Modulation of the ca2+ sensitivity of airway smooth muscle cells in murine lung slices. *American journal of physiology. Lung cellular and molecular physiology*, 291:L208–L221, 2006.

[5] A. Bergner and M.J. Sanderson. Acetylcholine-induced calcium signaling and contraction of airway smooth muscle cells in lung slices. *Journal of General Physiology*, 119:187–198, 2002.

[6] C.M. Bidan, A.C. Veldsink, H. Meurs, and R Gosens. Airway and extracellular matrix mechanics in copd. *Frontiers in Physiology*, 6:346, 2015.

[7] Y. Bossé, D. G. Chapman, P. D. Paré, G. G. King, and C. M. Salome. A 'good' muscle in a 'bad' environment: The importance of airway smooth muscle force adaptation to airway hyperresponsiveness. *Respir Physiol Neurobiol*, 179:269–275, 2011.

[8] C. E. Brightling, S. Gupta, S. Gonem, and S. Siddiqui. Lung damage and airway remodelling in severe asthma. *Clinical & Experimental Allergy*, 42:638–649, 2012.

[9] B.S. Brook, S.E. Peel, I.P. Hall, A.Z. Politi, J. Sneyd, Y. Bai, M.J. Sanderson, and O.E. Jensen. A biomechanical model of agonist-initiated contraction in the asthmatic airway. *Respir Physiol Neurobiol*, 170(1):44 – 58, 2010.

[10] C. Dassow, L. Wiechert, C. Martin, S. Schumann, G. Muller-Newen, O. Pack, J. Guttmann, W. A. Wall, and S. Uhlig. Biaxial distension of precision-cut lung slices. *Journal of Applied Physiology*, 108:713–721, 2010.

[11] N. Davidovich, J. Huang, and S. S. Margulies. Reproducible uniform equibiaxial stretch of precision-cut lung slices. *American journal of physiology. Lung cellular and molecular physiology*, 304:L210–L220, 2013.

[12] G. Farneback. *Image Analysis 13th Scandinavian Conference, SCIA 2003 Halmstad, Sweden, June 29 – July 2, 2003 Proceedings*, chapter Two-Frame Motion Estimation Based on Polynomial Expansion. Springer, 2003.

[13] R. Gosens and C. Grainge. Bronchoconstriction and airway biology: Potential impact and therapeutic opportunities. *Chest*, 147:798–803, 2015.

[14] H. D. Held, C. Martin, and S Uhlig. Characterization of airway and vascular responses in murine lungs. *British journal of pharmacology*, 126:1191–1199, 1999.

[15] J.E. Hiorns, O.E. Jensen, and B.S. Brook. Nonlinear compliance modulates dynamic bronchoconstriction in a multiscale airway model. *Biophysical Journal*, 107:3030–3042, 2014.

[16] J.E. Hiorns, O.E. Jensen, and B.S. Brook. Static and dynamic stress heterogeneity in a multiscale model of the asthmatic airway wall. *Journal of Applied Physiology*, 2016.

[17] A.L. James, T.R. Bai, T. Mauad, M.J. Abramson, M. Dolhnikoff, K.O. McKaye, P.S. Maxwell, J.G. Elliot, and F.H. Green. Airway smooth muscle thickness in asthma is related to severity but not duration of asthma. *Eur Respir J*, 34:1040–1045, 2009.

[18] T.L. Lavoie, R. Krishnan, H.R. Siegel, E.D. Maston, J.J. Fredberg, J. Solway, and M.L. Dowell. Dilatation of the constricted human airway by tidal expansion of lung parenchyma. *Am J Resp Crit Care*, 186(3):225–232, 2012.

[19] B. Ma, M.J. Sanderson, and J.H.T Bates. Airway- parenchymal interdependence in the lung slice. *Respir Physiol Neurobiol*, 185:211–216, 2013.

[20] D.T.K. Malcolm, P.M.F. Nielsen, P.J. Hunter, and P. Charette. Strain measurement in biaxially loaded inhomogeneous, anisotropic elastic membranes. *Biomechanics and Modelling in Mechanobiology*, 1:197–210, 2002.

[21] P. B. Noble, C. D. Pascoe, B. Lan, S. Ito, L.E.M. Kistemaker, A.L. Tatler, T. Pera, B. S. Brook, R. Gosens, and A.R. West. Airway smooth muscle in asthma: Linking contraction and mechanotransduction to disease pathogenesis and remodelling. *Pulmonary Pharmacology & Therapeutics*, 29:96–107, 2014.

[22] T.A. Oenema, H. Maarsingh, M. Smit, G.M.M. Groothuis, H. Meurs, and R. Gosens. Bronchoconstriction induces TGF-β release and airway remodelling in guinea pig lung slices. *PLoS ONE*, 8(6):e65580, 2013.

[23] J.F. Perez and M.J. Sanderson. The frequency of calcium oscillations induced by 5-HT, ACH, and KCl determine the contraction of smooth muscle cells of intrapulmonary bronchioles. *Journal of General Physiology*, 125:535–553, 2005.

[24] S. R. Rosner, S. Ram-Mohan, J. R. Paez-Cortez, T. L. Lavoie, M. L. Dowell, L. Yuan, X. Ai, A. Fine, W. C. Aird, J. Solway, J. J. Fredberg, and R. Krishnan. Airway contractility in the precision-cut lung slice after cryopreservation. *Am J Respir Cell Mol Biol*, 50:876–881, 2014.

[25] M. J. Sanderson. Exploring lung physiology in health and disease with lung slices. *Pulmonary Pharmacology & Therapeutics*, 24:452–465, 2011.

[26] M. Schleputz, A. D. Rieg, S. Seehase, J. Spillner, A. Perez-Bouza, T. Braunschweig, T. Schroeder, M. Bernau, V. Lambermont, C. Schlumbohm, K. Sewald, R. Autschbach, A. Braun, B. W. Kramer, S. Uhlig, and C. Martin. Neurally mediated airway constriction in human and other species: a comparative study using precision-cut lung slices (pcls). *PLoS ONE*, 7:e47344, 2012.

[27] M. Schleputz, S. Uhlig, and C. Martin. Electric field stimulation of precision-cut lung slices. *Journal of Applied Physiology*, 110:545–554, 2011.

[28] S. Seehase, M. Schleputz, S. Switalla, K. Matz-Rensing, F. J. Kaup, M. Zoller, C. Schlumbohm, E. Fuchs, H. D. Lauenstein, C. Winkler, A. R. Kuehl, S. Uhlig, A. Braun, K. Sewald, and C. Martin. Bronchoconstriction in nonhuman primates: a species comparison. *Journal of Applied Physiology*, 111:791–798, 2011.

[29] X. Tan and M.J. Sanderson. Bitter tasting compounds dilate airways by inhibiting airway smooth muscle calcium oscillations and calcium sensitivity. *British Journal of Pharmacology*, 171:646–662, 2014.

[30] I. Wang, A.Z. Politi, N. Tania, Y. Bai, M.J. Sanderson, and J. Sneyd. A mathematical model of airway and pulmonary arteriole smooth muscle. *Biophys J*, 94(6):2053 – 2064, 2008.

[31] A.R. West, N. Zaman, D.J Cole, M.J. Walker, W.R. Legant, T. Boudou, C.S. Chen, J.T. Favreau, G.R. Gaudette, E.A. Cowley, and G.N. Maksym. Development and characterization of a 3d multicell microtissue culture model of airway smooth muscle. *Am J Physiol Lung Cell Mol Physiol*, 304:L4–L16, 2013.

[32] A. Wohlsen, C. Martin, E. Vollmer, D. Branscheid, H. Magnussen, W. M. Becker, U. Lepp, and S. Uhlig. The early allergic response in small airways of human precision-cut lung slices. *European Respiratory Journal*, 21:1024–32, 2003.
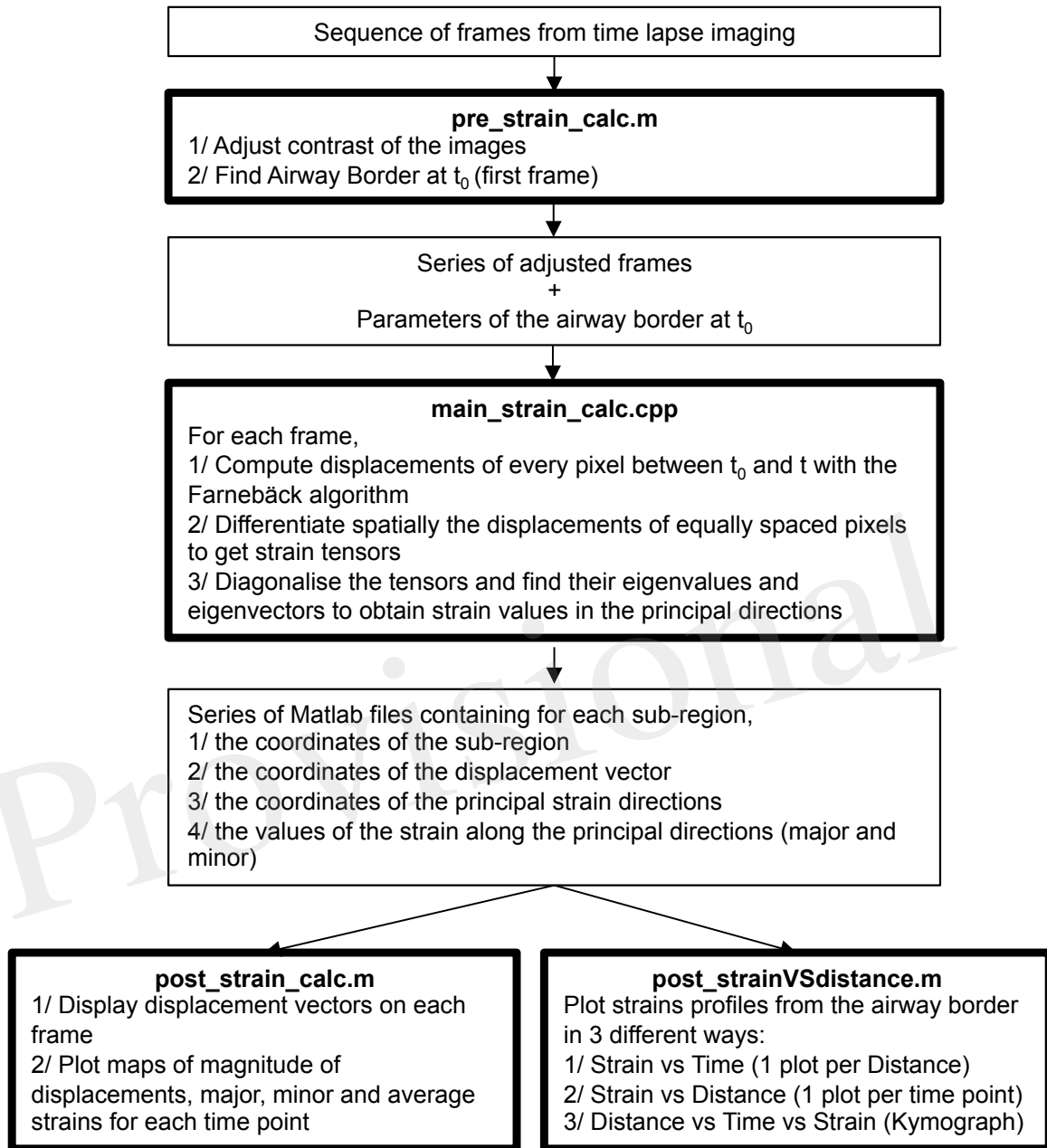
A-1 Appendix

A-1.1 Overview of image analysis

Figure A-1: Workflow showing steps required to compute global strain maps

A-1.2 Specific algorithms

A-1.2.1 Lumen edge detection

Having received the data in the form of videos, the free software Virtualdub (see www.virtualdub.org)
is used to save the individual frames. The image processing toolbox in MATLAB is used

20

```
┌─────────────────────────────────────────────────────────────┐
│        Sequence of frames from time lapse imaging             │
└─────────────────────────────────────────────────────────────┘
                              │
                              ▼
┏━━━━━━━━━━━━━━━━━━━━━━━━━━━━━━━━━━━━━━━━━━━━━━━━━━━━━━━━━━━━━━━━━┓
┃                      pre_strain_calc.m                        ┃
┃  1/ Adjust contrast of the images                             ┃
┃  2/ Find Airway Border at $t_0$ (first frame)                 ┃
┗━━━━━━━━━━━━━━━━━━━━━━━━━━━━━━━━━━━━━━━━━━━━━━━━━━━━━━━━━━━━━━━━━┛
                              │
                              ▼
┌─────────────────────────────────────────────────────────────┐
│                 Series of adjusted frames                     │
│                            +                                  │
│          Parameters of the airway border at $t_0$             │
└─────────────────────────────────────────────────────────────┘
                              │
                              ▼
┏━━━━━━━━━━━━━━━━━━━━━━━━━━━━━━━━━━━━━━━━━━━━━━━━━━━━━━━━━━━━━━━━━┓
┃                  main_strain_calc_spokes.cpp                  ┃
┃  For each frame,                                              ┃
┃  1/ Define a set of points in 8 spokes around the airway      ┃
┃  2/ Compute displacements of every pixel between $t_0$ and t  ┃
┃  with the Farnebäck algorithm                                 ┃
┃  3/ Use linear interpolation on the for nearest pixels to     ┃
┃  find displacement at the desired points                      ┃
┃  4/ Differentiate spatially the displacements to get strain   ┃
┃  tensors in those points                                      ┃
┃  5/ Diagonalise the tensors and find their eigenvalues and    ┃
┃  eigenvectors to obtain strain values in the principal        ┃
┃  directions                                                   ┃
┗━━━━━━━━━━━━━━━━━━━━━━━━━━━━━━━━━━━━━━━━━━━━━━━━━━━━━━━━━━━━━━━━━┛
                              │
                              ▼
┌─────────────────────────────────────────────────────────────┐
│  Series of Matlab files containing for each spoke,            │
│  1/ the distance of the points from the airway               │
│  2/ the average and standard deviation of the radial and     │
│  azimuthal displacements on all the points of a spoke at the  │
│  same distance from the airway                                │
│  3/ the average and standard deviation of the major, minor,   │
│  and average strain on all the points of a spoke at the same  │
│  distance from the airway                                     │
└─────────────────────────────────────────────────────────────┘
              │                              │
              ▼                              ▼
┏━━━━━━━━━━━━━━━━━━━━━━━━━━━┓    ┏━━━━━━━━━━━━━━━━━━━━━━━━━━━━━━━━┓
┃ post_strain_calc_spokes.m ┃    ┃ post_strainVSdistance_spokes.m┃
┃ Plot the profiles         ┃    ┃ Plot Distance vs Time vs Strain┃
┃ 1/ Average Strain vs      ┃    ┃ (kymograph) for each spoke     ┃
┃ Distance at different     ┃    ┗━━━━━━━━━━━━━━━━━━━━━━━━━━━━━━━━┛
┃ time points for each spoke┃
┃ 2/ Average strain with    ┃
┃ standard deviation        ┃
┃ vs Distance at desired    ┃
┃ time points for each      ┃
┃ spoke                     ┃
┗━━━━━━━━━━━━━━━━━━━━━━━━━━━┛
```
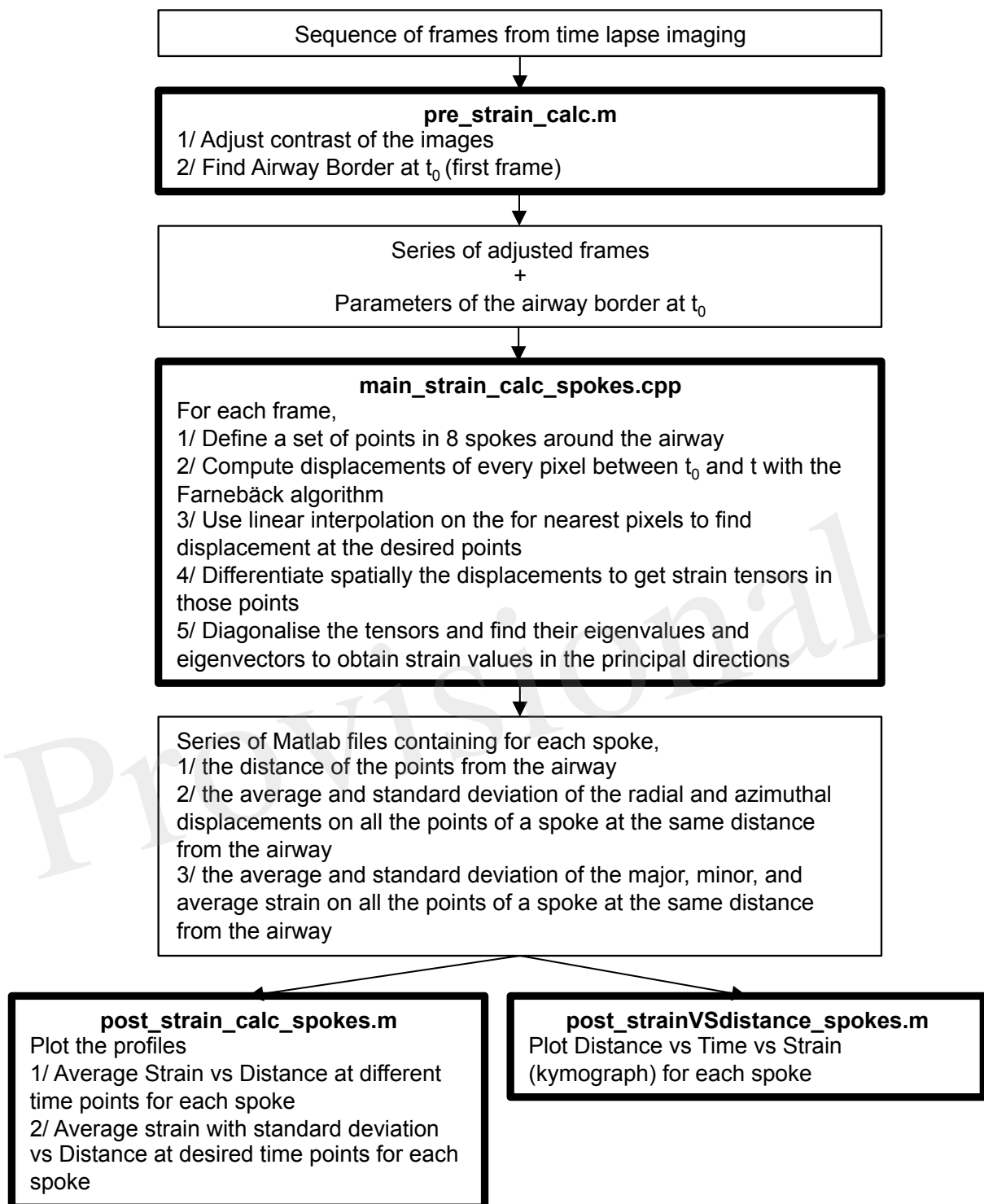
Figure A-2: Workflow showing steps required to compute strain maps along user-specified spokes.

to detect the edge, and the area, of the lumen in each frame. Depending on the lung slice being considered, specific MATLAB procedures are used in each of the frames; the image processing tools used in the procedures are detailed further, and the code is provided, in the Supplementary Material.

In each of the two methods we developed, an estimate for the edge of the lumen is determined, which can also be used to determine the lumen area either directly or by fitting an ellipse to the lumen. For the PCLS that had a clear contrast between the lumen and the airway wall we used the following sequence of tools: (i) `imread`, `imcrop`; (ii) `graythresh`, `im2bw`; (iii) `bwareaopen`; (iv) `imfill`; (v) `bwconncomp`, `regionprops`. From `regionprops` we obtain two estimates for the area of the lumen at each frame. An area can either be calculated within the region found (using `pwperim`) or an ellipse can be fitted to the region.

An alternative method for lumen edge detection (if the contrast between lumen and airway is not sufficient) uses the following sequence of MATLAB tools: (i) `imread`, `imcrop`, `rgb2gray`, `edge(I,'canny', thresh)`; (ii) `imdilate(I, [se90 se0])` (this closes the gaps between the edges that have been found); (iii) `imcomplement`, `bwareaopen`; (iv) `imfill`; (v) the area of the region detected, or that within a fitted ellipse, can be found using `bwconncomp` and `regionprops`.

A-1.2.2 Farnebäck method

The Farnebäck algorithm [12] as implemented in the opencv code cv::calcOpticalFlowFarneback[1], was used to calculate an estimate of the displacement vector between an initial and final image, for each of the pixels. In order to make the features in each of the images more prominent, prior to using the algorithm, the contrast of each image was increased. Each of the images was converted to greyscale and the range of the pixel intensities was stretched so that 1% of the pixels were saturated at the brightest value and 0.01% were saturated at the darkest value. The following MATLAB commands were used to do this: `imread`, `rgb2gray`, `stretchlim`, `imadjust` and `imwrite`. In regions where not enough features and/or insufficient contrast remained, thresholds were set to recalculate the displacements of the corresponding pixels by interpolation. This avoided the computation of spurious displacements. For any such points, the displacement was first set to `NAN` and then `griddata` in MATLAB was used with the `v4` method, to update the displacement at each of these points.

Following [12], we suppose that the two images are approximated by quadratic polynomial functions that describe the intensity of the pixels at position $\mathbf{x}$. The polynomials for the first and second image have the form

$$f_1(\mathbf{x}) = \mathbf{x}^T A_1 \mathbf{x} + \mathbf{b}_1^T \mathbf{x} + c_1, \tag{A-1}$$

$$f_2(\mathbf{x}) = \mathbf{x}^T A_2 \mathbf{x} + \mathbf{b}_2^T \mathbf{x} + c_2, \tag{A-2}$$

where A_1, A_2 are 2x2 matrices, $\mathbf{b}_1$, $\mathbf{b}_2$ are 2x1 vectors and c_1, c_2 are scalars. If the two images are only different by a rigid shift, $f_1(\mathbf{x}) = f_2(\mathbf{x} - \mathbf{d})$, where $\mathbf{d}$ is the displacement of the shift to be found. In this case

$$A_2 = A_1, \quad \mathbf{b}_2 = \mathbf{b}_1 - 2A_1\mathbf{d}, \quad c_2 = \mathbf{d}^T A_1 \mathbf{d} - \mathbf{b}_1^T \mathbf{d} + c_1, \tag{A-3}$$

---

[1]http://opencv.willowgarage.com/documentation/cpp/motion_analysis_and_object_tracking.html

where, assuming that A_1 is non-singular, $\mathbf{d}$ is given by

$$\mathbf{d} = -A_1 \frac{\mathbf{b}_2 - \mathbf{b}_1}{2}. \tag{A-4}$$

In general it is more complicated than this, since the displacement is spatially dependent and will also involve rotation and stretching. Rather than finding intensity polynomial functions over the whole region, local polynomial functions are found over a small neighbourhood surrounding each of the pixels. A spatially-dependent displacement $\mathbf{d}(\mathbf{x})$ is found using the local polynomials of the two images. If however, the displacements are large, the comparison of local polynomials in the two images may be insufficient, since the displaced point may not be located within the local neighbourhood of the initial position used to form the polynomial. In this case a false displacement will be found. The algorithm is able to overcome this problem by using *a priori* knowledge. Given an *a priori* displacement $\tilde{\mathbf{d}}(\mathbf{x})$, a relative displacement can be found using $f_1(\mathbf{x})$ and $f_2(\tilde{\mathbf{x}})$, where $\tilde{\mathbf{x}} = \mathbf{x} + \tilde{\mathbf{d}}(\mathbf{x})$. $\tilde{\mathbf{d}}(\mathbf{x})$ (which is measured relative to pixel width) is rounded to the nearest integer, so that the polynomial in the second image is centred on a pixel. Now in general, $A_1 \neq A_2$, but introducing

$$A(\mathbf{x}) = \frac{A_1(\mathbf{x}) + A_2(\tilde{\mathbf{x}})}{2}, \quad \Delta\mathbf{b}(\mathbf{x}) = -\frac{1}{2}(\mathbf{b}_2(\tilde{\mathbf{x}}) - \mathbf{b}_1(\mathbf{x})) + A(\mathbf{x})\tilde{\mathbf{d}}(\mathbf{x}), \tag{A-5}$$

the constraint for the updated displacement is

$$A(x)\mathbf{d}(\mathbf{x}) = \Delta\mathbf{b}(\mathbf{x}). \tag{A-6}$$

In practice the displacement field that is found will be too noisy. The algorithm overcomes this by assuming that the displacement field is only slowly varying. In this case, for each pixel, it is possible to solve with an appropriate weight function $w(\Delta\mathbf{x})$ over a region Ω, which forms a square of pixels around the current pixel. This results in having to find the minimum of

$$\sum_{\Delta\mathbf{x}\in\Omega} w(\Delta\mathbf{x})\|A(\mathbf{x} + \Delta\mathbf{x})\mathbf{d}(\mathbf{x}) - \mathbf{b}(\mathbf{x} + \Delta\mathbf{x})\|^2. \tag{A-7}$$

Increasing the size of Ω results in smoother displacement fields.

In reality an initial guess of the displacements was generally not available, in which case an iterative system could be used. The initial iterations were used to find an approximation of the displacements, with further iterations improving the approximation. If the displacement between the two frames was large, the initial size of the neighbourhood, used to fit the polynomials $f_1(\mathbf{x})$ and $f_2(\mathbf{x})$, was increased, in order to find a rough but reasonable displacement estimation. This displacement was then used as a priori displacement, which was improved in two ways. Further iterations were carried out with the same neighbourhood size, or in order to find more of the local features of the displacement field, the size of the neighbourhood of the pixels used to find the polynomials was reduced.

When implementing the OpenCV code, unless otherwise stated we used three sizes of square neighbourhoods to form the pixel intensity polynomials. For each subsequent square size we halved the length of sides and iterated three times for each size. Using the suggested values in the OpenCV documentation, we used a final side length of 5 pixels and set the standard deviation of the Gaussian, used to smooth derivatives in order to form the polynomials $f_1(\mathbf{x})$ and $f_2(\mathbf{x})$, to 1.1 pixels. However this had to be modified to 7 and 1.5 (still following the OpenCV documentation) to track large displacements on high resolution pictures (1280x960 pixels). We found that introducing additional larger squares

23

did not improve the results.

A-1.2.3 Determining displacements for points along normal vectors

An alternative to calculating the entire displacement field was to find the displacement at selected points. By selecting points along a normal vector to the lumen, it was easier to quantify displacement as a function of radius (or distance from the lumen). By doing this at various points around the lumen, the displacement-radius relationship could be compared. We first fitted an ellipse to the lumen at the start of the contraction (details in S. in Supp. Mat). We then split the airway into eight sections, within each of which we selected points along normal vectors starting at seven points on the lumen boundary. We found displacements in the tangential and normal directions at each point and averaged these values within each of the sections for each radial position, in order to remove small errors.

We begin by fitting an ellipse to the lumen at the start of the contraction, using the techniques described in section A-1.2.1. In parametric form an ellipse centred at (x_0, y_0), with major and minor axis of length $2a$ and $2b$ and angle α between the x axis and the major axis, has coordinates

$$x = x_0 + a \cos t \cos \alpha - b \sin t \sin \alpha, \tag{A-8a}$$

$$y = y_0 + a \cos t \sin \alpha + b \sin t \cos \alpha, \tag{A-8b}$$

where $t \in [0, 2\pi)$ is the parametric parameter. The unit vectors in the tangential and normal directions are

$$\mathbf{t} = \frac{(-a \sin t \cos \alpha - b \cos t \sin \alpha, -a \sin t \sin \alpha + b \cos t \cos \alpha)}{\sqrt{a^2 \sin^2 t + b^2 \cos^2 t}}, \tag{A-9a}$$

$$\mathbf{n} = \frac{(-a \sin t \sin \alpha + b \cos t \cos \alpha, a \sin t \cos \alpha + b \cos t \sin \alpha)}{\sqrt{a^2 \sin^2 t + b^2 \cos^2 t}}. \tag{A-9b}$$

Eight groups of seven points are chosen on the ellipse with the coordinates

$$(x_e, y_e) = (x(t), y(t)), \quad t = \alpha + m\pi/4 + n\pi/180, \tag{A-10}$$

with $m = 0, 1, .., 7$ and $n = -3, -2, .., 3$. If the ellipse was a perfect fit to the lumen each of the points would be located at the lumen boundary. In practice the lumen is not so regular, so the choice of points given in (A-10) may need to be slightly altered. Where required, we slightly inflate or deflate the ellipse, while fixing the ratio of a and b, in order to select a point on the boundary. For each of the new points we find the normal to the lumen and select further points spaced by k pixels in the direction of the normal. This yields the points

$$(x, y) = (x_e, y_e) + \mathbf{n}(t)ks, \quad s = 0, 1, ... \tag{A-11}$$

An illustration of how one line of points are chosen and an example of the points chosen is shown in Fig. A-3. Since in general the coordinates are not integer values, bilinear interpolation of the four nearest pixels is used to find the displacement. The radial and azimuthal components of the displacements are found by taking the dot product of the displacement with the unit normal and tangent vectors.
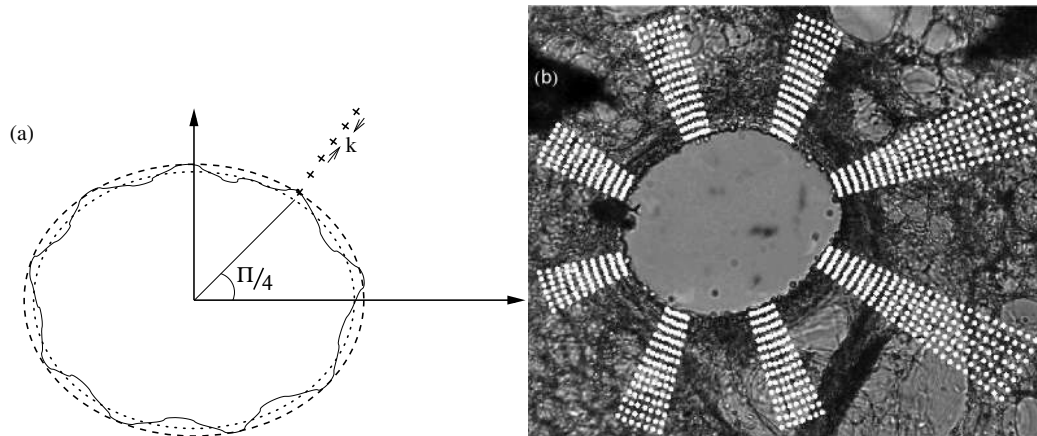
Figure A-3: (a) An ellipse (dotted line) is fitted to the edge of the lumen (solid line). However, a particular point on the lumen boundary may not lay on this ellipse, in which case we inflate (or deflate) the ellipse accordingly so that the point lies on the adjusted ellipse (dashed line). The normal to the adjusted ellipse is found and points are chosen at intervals of k pixels. (b) An example of the initial set of points (white dots) superimposed on an image of a lung slice.

A-1.3   Lumen area image processing tools

The following tools are used in at least one of the procedures (`I` is used to represent the latest version of the image):

- `imread(N)`: used to load up the image from a file N;

- `imcrop(I, rect)`: used to take a rectangular section (`rect` specifies the coordinates of the section) of the image around the airway;

- `level = graythresh(I)`: computes a threshold of the image, which can be used to produce a binary image;

- `im2bw(I,level)`: changes the image to a binary image;

- `rgb2gray(I)`: converts an image to greyscale;

- `bwareaopen(I, numpixel, 4)`: removes from the binary image any groups of less than numpixel of connected pixels (4 means that two pixels are only connected if they share an edge);

- `imfill(I,'holes')`: fills in any small holes in an object;

- `edge(I,'canny', thresh)`: detects edges using the Canny method (Edges are found by searching for local maxima of the gradient of `I`. The derivative of a Gaussian filter is used to calculate the gradient. The method uses two thresholds, to detect strong and weak edges, only including the weak edges if they are connected to strong edges.);

- `imdilate(I, [strel('line', 3, 90) strel('line', 3, 0)])`: lines are dilated by three pixel each way in the horizontal and vertical directions;

- `imcomplement(I)`: the binary image is inverted;

25

644 ● `cc = bwconncomp(I,4)`: the binary image is split up into sections depending
645 on the connectivity of the pixels (the resulting number of objects can be obtained
646 using `cc.NumObjects`);

647 ● `imagedata = regionprops(cc, 'Area', 'Centroid', 'Orientation',`
648 `'MajorAxisLength', 'MinorAxisLength')`: finds the area and centroid
649 of each object and the length of the major and minor axis and the orientation of the
650 major axis to the horizontal of an ellipse that has the same second-moments as the
651 object;

652 ● `BWoutline = bwperim(I); Segout = I2; Segout(BWoutline) = 255`:
653 draws the outline found onto the original image.